Experimental investigation of an autonomous flap for load alleviation

Bernhammer, Lars O.; Navalkar, Sachin T.; Sodja, Jurij; De Breuker, Roeland; Karpel, Moti

DOI
10.2514/6.2015-1852

Publication date
2015

Published in
Proceedings 56th AIAA/ASCE/AHS/ASC Structures, Structural Dynamics, and Materials Conference

AIAA SciTech Forum
5-9 January 2015, Kissimmee, Florida
56th AIAA/ASCE/AHS/ASC Structures, Structural Dynamics, and Materials Conference

10.2514/6.2015-1852

Experimental investigation of an autonomous flap for load alleviation

Lars O. Bernhammer* and Sachin T. Navalkar † and Jurij Sodja ‡ and Roeland De Breuker§
Delft University of Technology, Delft, 2629HS, The Netherlands

Moti Karpel¶
Technion Israel Institute of Technology, Haifa, 32000, Israel

This paper presents an experimental aeroservoelastic investigation of a novel load alleviation concept using trailing edge flaps. These flaps are autonomous units, which are self-powered and self-actuated, using trailing edge tabs, thereby demonstrating advantages in comparison with conventional flap systems in terms of wiring and structural integration. The flaps are free-floating and mass underbalanced, such that they may flutter at operation velocities unless suppressed by their own control system. This makes the system very responsive for turbulence and control action. In the wind tunnel campaign presented in this paper, the limit cycle behavior of autonomous, free-floating flaps was investigated. It has been shown that limit cycle oscillation can be reached either through structural limiters or by control actions of the trailing edge tabs. In the latter case, the amplitude of the limit cycle oscillation is adjustable to the required energy output. An energy balance of harvested power and power consumption for actuators and sensing system was made showing that the vibration energy of limit cycle oscillations can be used to keep the amplitude of the limit cycle constant, while the electric batteries that power the load alleviation system are being charged.

Keywords: Autonomous free-floating flap, aeroelastic instability, wind tunnel experiments

I. Introduction

A design driver in the structural design of aircraft wings and wind turbine blades are gust encounters and turbulence. A concept that can help reducing these dynamic loads are actively controlled trailing edge flaps. Flaps are particularly suitable because of their high control authority and their high frequency bandwidth. One of the possible flap designs employs free-floating flaps (FFF), which can freely rotate around a hinge axis and are controlled by trailing edge tabs. Heinze and Karpel[1] have first investigated this concept by using a single FFF to control very flexible wings. The study was followed-up by Bernhammer et al.,[2] who investigated flutter suppression and gust load alleviation on a vertical tail plane using FFF. Pustilnik and Karpel[3,4] performed numerical studies on limit cycle oscillation based on the experiment of Bernhammer et al.[2]

For the current research, the control function of the free-floating flap is expanded by a secondary purpose, namely energy harvesting as proposed by Bernhammer, De Breuker and Karpel.[5] Energy harvesting from mechanical vibrations is widely studied, however exploiting aeroelastic instabilities for energy generation is not well-researched yet. First work in this field has been done by Bryant and Garcia[6] and Bryant, Fang and Garcia[7] by investigating the power production during flutter of a piezoelectric sheet embedded in a cantilever beam with a free-floating flap at its end. Their experiments were complimented by a a numerical study exploiting 2 dimensional unsteady aerodynamics coupled to a structural model with 2 degree of freedom. It

*PhD Candidate, Aerospace Structures and Computational Mechanics/ Wind Energy
†PhD Candidate, Delft Center for Systems and Control
‡Aerospace Structures and Computational Mechanics
§Assistant Professor, Aerospace Structures and Computational Mechanics
¶Professor, Sanford Kaplan Chair for Aerospace Engineering, Fellow AIAA

was demonstrated how changing the mass and stiffness distribution influences the system behaviour. Park et al.[8,9] exploit electromagnets to convert the vibrational energy to electrical energy. Instead of using a coupled flutter mechanism of the free-floating flap as Bryant and Garcia,[6] they use a T-shaped cantilever beam. From the end plate vortices are shed, which leads to a 1 degree of freedom flutter. The magnet is attached at the free tip and generates a magnetic field that induces currents in the coils that are place in a non-translating frame. Bernhammer, Karpel and De Breuker[5] integrated generators into 2 free-floating flaps in a tailplane.

The integration of both control and harvesting application into a single device has been proposed by Bernhammer et al.[10] In their paper the design of an autonomous, free-floating flap for load alleviation purposes in wind tunnel experiments is described. The current paper presents the experimental results of the measurement campaign using autonomous flaps. First, an overview of the autonomous flap concept is presented, then the design of the wind tunnel model is summarized. The Open Jet Facility of Delft University of Technology is shortly introduced. The wind tunnel measurements are started with a system identification and a comparison thereof to the numerically obtained system.[10] A controller has been design and it is demonstrated how such a controller can suppress flutter or bring the system to a stable limit cycle. Finally an analysis of the energy balance of the actuation and sensing system to the power generation of the flaps is made.

II. Concept of the Autonomous Flap

Autonomous flaps combine the functionality of the free-floating flap with an energy harvester. The autonomous flap concept is detailed in Figures 1 and 2. The flap is the top level component, which contains all subcomponents such as sensors, a control system, actuators, an energy harvesting device and the trailing edge tab. The most significant advantage of the autonomous flap is that is a completely autarkic system, meaning that no connection to the wing or blade structure is needed other than an a structural attachment. It can be used as plug and play device on existing structures.

One or multiple sensors (accelerometers in this paper) measure the motion of the wing-flap system. As shown in Figure 2 the accelerometer should be mounted close to the rotational axis of the flap such that the plunge motion of the wing is dominant in the measured acceleration response. The obtained signal is used as input to a controller, which has been developed based on an experimental system identification of the autonomous, free-floating flap in the aeroelastic apparatus. The controller sets the deflection angle of the trailing edge tab by commanding the actuator. An aerodynamic moment is generated by the trailing edge tab that rotates the flap.

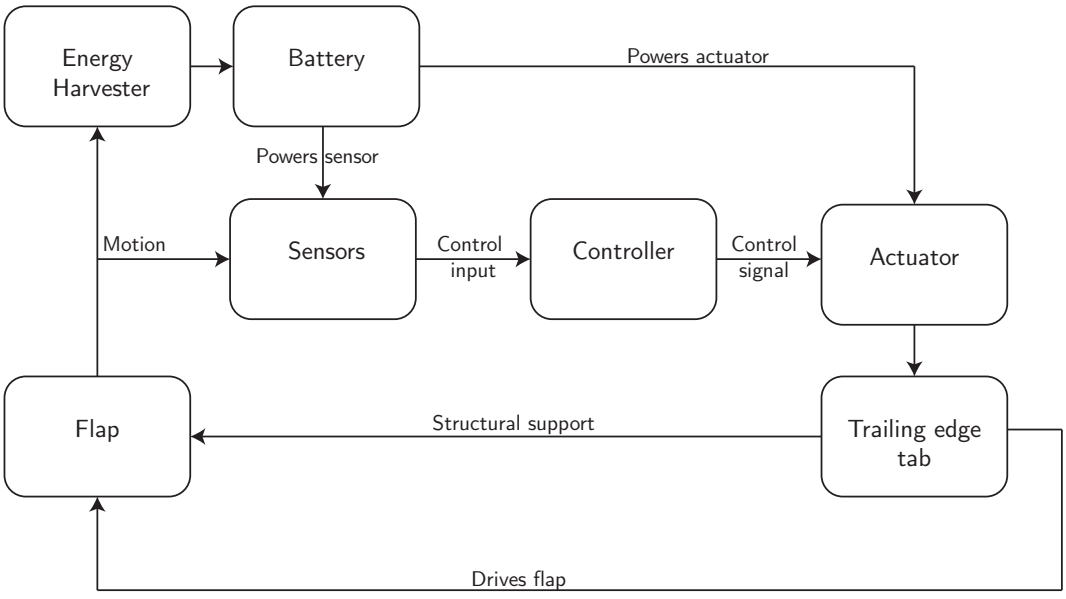

Figure 1: Flow chart of autonomous flap concept[10]

The sensors, the control system and the actuation system is powered by electromagnetic harvesting of the vibrations. As has been shown,[5] the power generation is particularly effective when the system is aeroelastically instable. It is highly interesting to generate controlled oscillations that can provide a continuous power production without being destructive for the structure. A potential solution are limit cycle oscillations (LCO). The amplitude of such oscillations can be limited either structurally or actively by the controller.

A second reason why it is desirable to have the free-floating flaps operating close to the flutter point is that the effective inertia of the flaps is reduced due to unsteady aerodynamic forces. The free-floating flap can be very efficiently controlled by the trailing edge tab as the gear ratio between the control input and the flap deflection strongly increases when approaching flutter speed.[2] This high gear ratio reduces the required trailing edge angles and therefore also the requirements to power the actuators.

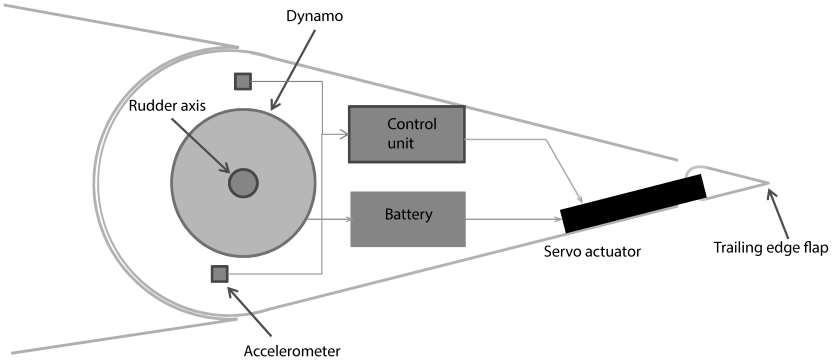

Figure 2: Schematic build-up of autonomous flap[10]

III. Aeroelastic Test Set-Up

A. Aeroelastic Apparatus

The autonomous, free-floating flap concept was integrated in an aeroelastic apparatus of a wing that can undergo pitch and plunge motion. This test set-up has been heavily validated for conventional flap systems using CFD data.[11] The aeroelastic apparatus is displayed in Figure 3. The wing model (F) is attached by springs to a frame built of sidewalls (C) connected by beams (D). This frame is mounted on a table (B), which can be adjusted to the height of the jet exit of the open test section (A). Struts (E) on both sides are used to increase the stiffness of the frame. Plunge and pitch motion of the wing are decoupled by having a global translating system (I) on which rotational springs are mounted that give an additional degree of freedom as shown in Figure 4. The side plates are guided by a rail system to prevent motion other than pure plunge. The properties of this set-up are given in Table 1. The springs (H) are attached to load cells and the side plates (I) are equipped with angular sensors and accelerometers. Strain gauges are attached to the root of the wing section.

B. Autonomous Flap Design

The detailed design of the autonomous, free-floating flap model was presented by Bernhammer et al.[10] Table 2 provides an overview of the equipment that has been installed in the autonomous flap. The arrangement of all components in the flap is shown in Figure 5. The accelerometer (A) measures motion in the plunge direction. The potentiometers (B) and the gear boxes (C) serve as hinges with the main wing. The gear box is connected to a generator, in which the rotor is the magnet and the stator is the coil. A pair of servo-motors (D) drives the trailing edge tab (E).

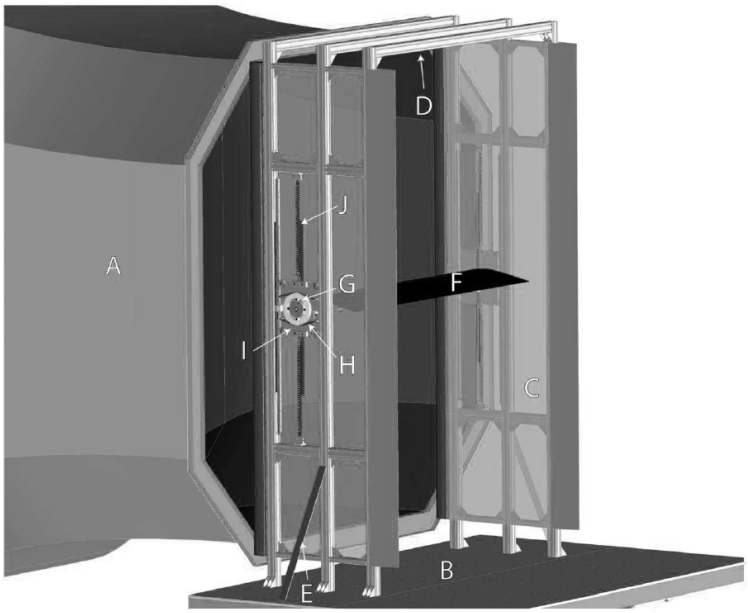

Figure 3: Experimental set-up in open jet facility: the jet exit (A), the table (B), two sides upright (C), connecting beams (D), struts (E) and the wing (F). Moment sensors (G) are attached to springs (H) on movable side plates (I)[11]

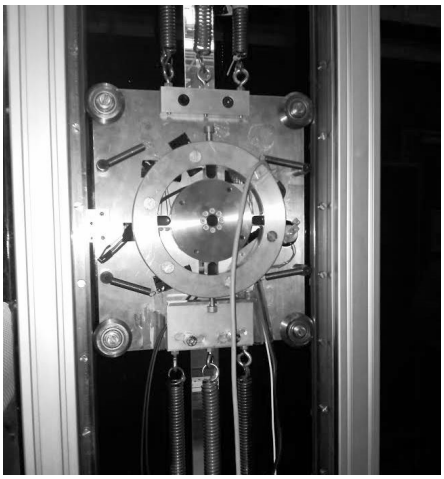

Figure 4: Plunge-pitch mechanism

Table 1: Properties of aeroelastic set-up

Width	1800 mm
Chord	500 mm
Airfoil profile	DU96-W-180
Flap length	100 mm
Plunge spring stiffness	8225 N/m^2
Structural damping	77.9 kg/s
Wing assembly mass	22.7 kg
Wing mass	15.2 kg
Side plate mass	7.5 kg
Eigenfrequency	3.0 Hz

Table 2: Flap design parameters

Material	SL-Tool STONElike[a]
Density	1.37 g/cm^3
Young's modulus	3.5 GPa
Tensile strength	47 MPa
Skin thickness	2 mm
Servo actuator	HiTech HS-7115TH[b]
Gear box	Apyxdyna AM022 [c]
Gear ratio	1:80
Generator	Kinetron MG 23.0[d]
Analogue devices	ADXL78[e]

[a] https://www.robotmech.com/uploads/media/robotmech-SL-TOOL-Stonelike_EN.pdf

[b] http://hitecrcd.com/products/servos/premium-digital-servos/hs-7115th-hv-ultra-slim-titanium-gear-servo/product

[c] http://www.apexdyna.nl/en/producten/am-series.html

[d] http://www.kinetron.eu/micro-generator-technology/

[e] http://www.analog.com/en/mems-sensors/mems-inertial-sensors/adxl78/products/product.html

C. Open Jet Facility

The experiment has been performed in the Open Jet Facility (OJF) of Delft University of Technology. This wind tunnel is has been designed for large scale models and is particularly suitable for unsteady aeroelastic investigations. The tunnel is a closed circuit design with a jet exit into the test section of 2.85m by 2.85m. Wind speeds up to 35 m/s can be reached, which correspond to Reynolds numbers of 1,230,000 based on a 50cm chord. This Reynolds number is lower than in aircraft or wind turbine applications, but high enough to eliminate viscous flow effects. The Reynolds number at the predicted flutter speed is 320,000 with at a reduced frequency of 0.136, which is well in the unsteady region and corresponds to the 3rd flapwise eigenfrequency in 5MW turbines.

IV. Aeroelastic Analysis

The model has been studied numerically. As a first step a flutter analysis has been performed. It is very critical to operate close to the flutter speed as both the control authority of the trailing edge tabs increases[2] as well as the power generation through energy harvesting.[5] The flutter analysis has been done in MSc Nastran using the PK-method.[12] Figure 6 shows the relevant aeroelastic modes. The frequencies in the

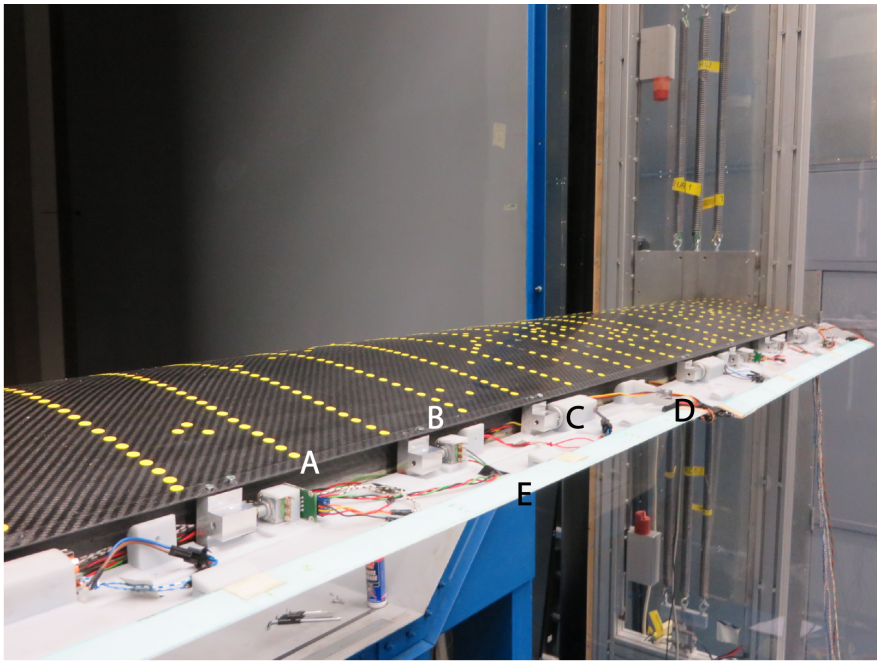

Figure 5: Free-floating flap with active trailing edge

caption of Figure 6 correspond to the natural frequencies without aerodynamics. The first two modes are rigid body modes of the free-floating flap at 0 Hz. The third eigenmode is a plunge dominated mode at 3 Hz, that also has a flap deflection component. The forth rigid body mode of wing is a torsional mode with a frequency of 6.8 Hz. All elastic wing modes are clearly separated in terms of frequency from the rigid body and flap modes. Their frequencies are more than an order of magnitude higher.

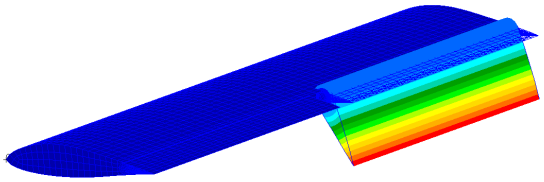

(a) 1st flap mode at 0 Hz

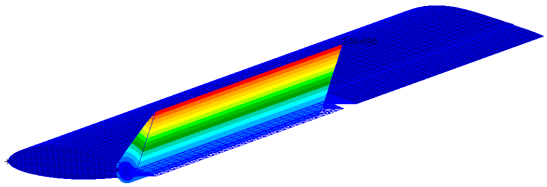

(b) 2nd flap mode at 0 Hz

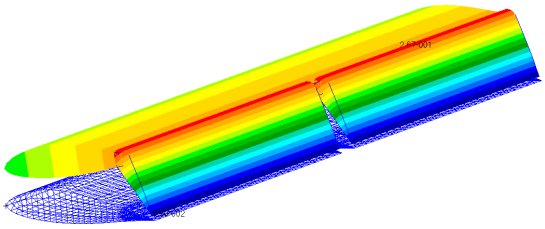

(c) 1st plunge mode at 3.0 Hz

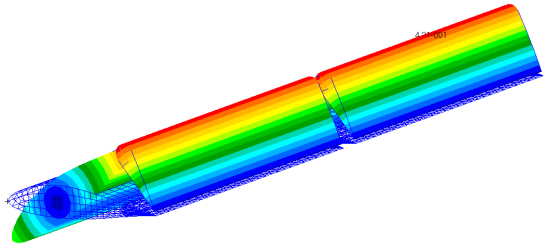

(d) 1st pitch mode at 6.8 Hz

Figure 6: Structural modes

The frequency and damping plots of the aeroelastic system are shown in Figure 7. The frequencies of the two flap modes increase almost linearly with the wind speed. Aerodynamic stiffness is added to the flap deflection modes, which results in an increase of the oscillation frequency. The flap deflection curve with the higher slope corresponds to a synchronous vibration of the two flaps, whereas the curve with the smaller

slope corresponds to a 180 degree phase difference between the two flaps. Both modes are highly damped. While the frequency of both flap deflection modes increases quickly with the velocity, the frequency of the plunge mode is constant up to 8 m/s. From that velocity onwards, interaction of the plunge mode with the synchronous flap deflection mode takes place and the damping of the plunge mode reduces until flutter occurs. The flutter speed can be found at a velocity of 11 m/s. Figure 8 shows 4 snapshots over a half-cycle of the unstable plunge mode at the flutter speed.

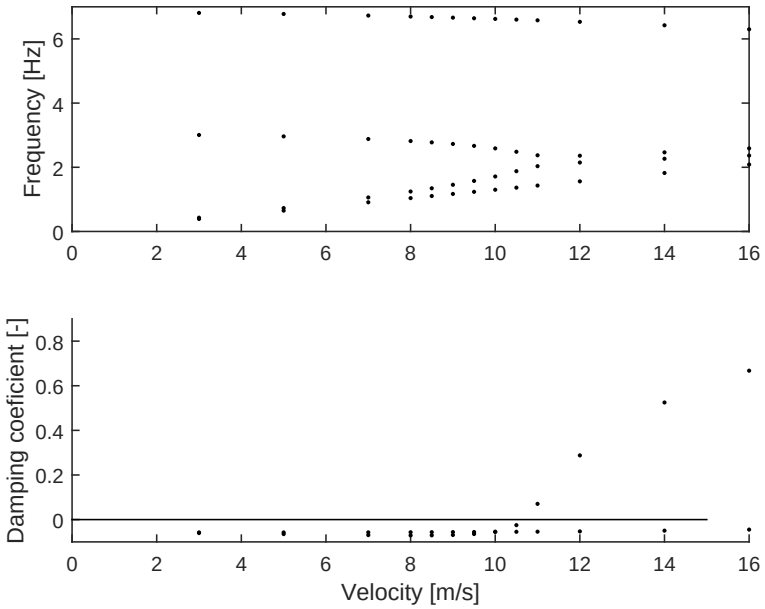

Figure 7: Damping and frequency plots as function of velocity

The frequency of the pitching mode hardly changes in the velocity window of the experiment up to 20 m/s. Around 30 m/s the frequency of the plunge mode drops from the natural frequency of 6.8 Hz to 5.0 Hz. At this point interaction with the plunge mode takes place, which has a frequency of 3.7 Hz. Quickly both modes approach each other in terms of frequency until they have the same frequency of 4.2 Hz at 40 m/s. This pitch-plunge type of flutter is however outside of the scope of the investigation.

As a final design step, the mode shapes as obtained by MSC Nastran have been used as basis for an aeroelastic analysis in ZAERO.[13] ZAERO has been used to obtain a state-space representation of the aeroelastic plant. The transfer functions between accelerometers and tab deflection angle have been assessed using the obtained state-space models for a velocity of 10 m/s. The Bode plots are given in Figure 9. Both eigenfrequencies of plunge and pitch modes are clearly visible at 2.6 Hz and 6.7 Hz, respectively. The acceleration of one of the two flaps is used as sensor. The 2 curves visible in Figure 9 correspond to trailing edge activity on the flap with the sensor and on other flap. For frequencies up to 20 Hz, the responses are identical. This is to be expected as both plunge and pitch motion are symmetric with respect to the midplane.

Compared to previous research[2] the control authority is reduced. The reason is that a smooth transition between wing and flap is desired. To achieve this, the hinge line has been moved forward to coincide with the end point of the main wing structure. This increases the moment arm to the aerodynamic center of the flap, thereby reducing the effectiveness of the trim tabs. Nonetheless, one degree of trim rotation still translates into 0.5 degrees of flap deflection.

V. Model Identification and Controller Design

The first step in the wind tunnel experiments was a system identification to design a control system for the autonomous flap. Due to friction in the flap mechanism of the wind tunnel model, the flutter speed was increased compared to the numerical studies, such that instabilities occured above 13 m/s. The exact flutter

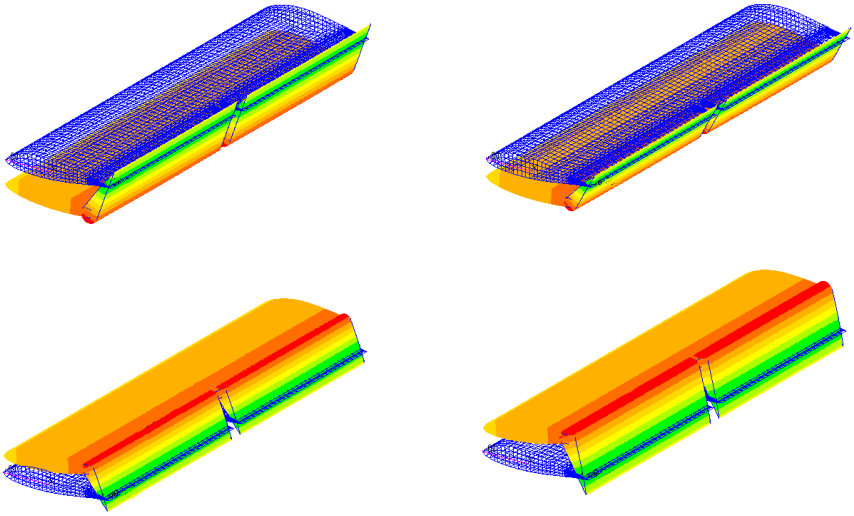

Figure 8: 4 snapshots of flutter mode over a half-cycle

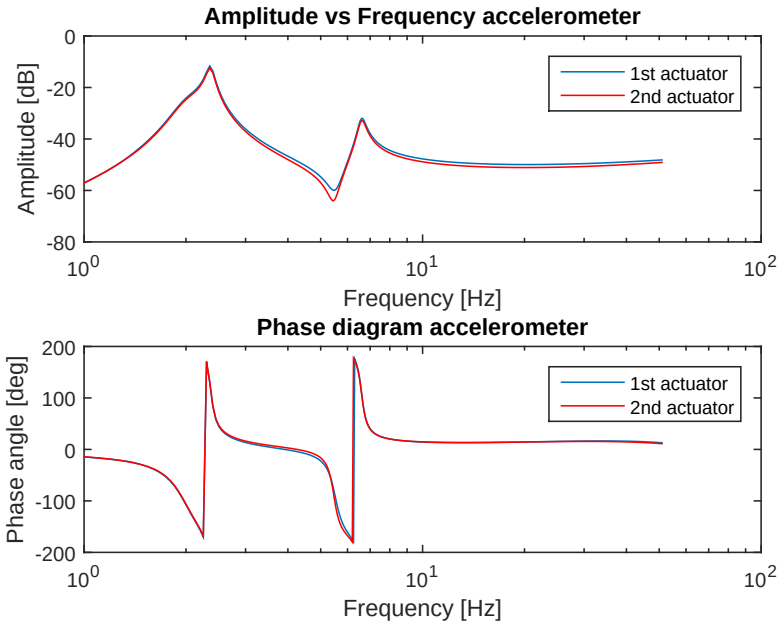

Figure 9: Transfer function of trim tab deflection to plunge acceleration

point could not be determined as the damping of the aeroelastic apparatus was highly non-linear for small vibration amplitudes. Once a vibration amplitude threshold was passed, the damping coefficient approached a value of 0.057, which was used in the numerical study.

In order to use the tabs for controlling structural vibrations, a feedback controller is required to be designed. This is done in two steps: first, system identification is used to arrive at a dynamic model of the system. Next, classical loop-shaping techniques are used to design a controller that is capable of damping the first vibrational mode of the system.

A. System Identification

One of the requirements for the design of a classical feedback controller is a simple dynamic model of the system to be controlled, preferably in terms of linear differential equations. Such a model may be obtained from first principles and physical modelling, but such models typically require high accuracy in experiment construction and calibration. With structural and aerodynamic non-linearities, the complexity of such physical models often renders them challenging for the purpose of controller synthesis. Further, they may involve dynamics that are irrelevant within the controller bandwidth.

An alternative approach to obtain a controller-relevant system model is to use system identification techniques, such as subspace identification.[14] In such a method, experimental data is obtained by exciting the system and the input-output data is used directly to estimate a dynamic system model that can be used for controller design. The decision was taken as the accelerometer mounted on the side planes was delivering a measurement signal with a significantly higher signal to noise ratio than the accelerometers in the flaps. Consequently, a less polluted system identification could be performed.

To simplify the identification problem, the identification experiment is conducted at a single wind speed (12.5 m/s) which is below the flutter speed, so that the system is stable and can be approximated as linear. The wing is excited by applying a pseudo-random binary sequence to the tabs, which results in structural oscillations. The structural vibrations are measured by the accelerometer located on the side-plates, which is the signal that will be used as feedback for the controller.

A transfer function $G(s)$ is estimated which describes the dynamics from the tab actuation angle β to the accelerometer response a_y, using the PBSID system identification technique.[15]

$$a_y = G(s)\beta. \tag{1}$$

The frequency-domain representation of the identified system is given in Figure 10

The solid green line is the actual frequency-domain data obtained from the experiment, while the solid blue line shows an estimate of the underlying system. As expected, a resonance peak at the first structural mode of 3.0 Hz is clearly identified in the system identification experiment. While the frequency of the instable branch of the numerical model decreases from the natural frequency of 3.0 Hz to 2.6 Hz when approaching the flutter speed, the experiment does not exhibit this behaviour. Only a slight decrease in frequency from 3.0 Hz to 2.9 Hz can be observed.

Using this identified model, a classical feedback controller is now designed for the system.

B. Controller Design

The structural vibrations measured by the accelerometer are fed back into the controller, which generates the appropriate tab actuation signal to counteract and thereby damp the vibrations. Hence, there are three major considerations for the controller:

- There must adequate gain around the first mode frequency of 3.0 Hz to be able to achieve feedback control.
- The actuation signal generated at the resonance frequency must produce an anti-phase structural response so that the vibrations are attenuated and not enhanced.
- The resulting closed-loop system must be stable.

Taking these considerations into account, a feedback controller $K(s)$ is designed that consists of the following three elements:

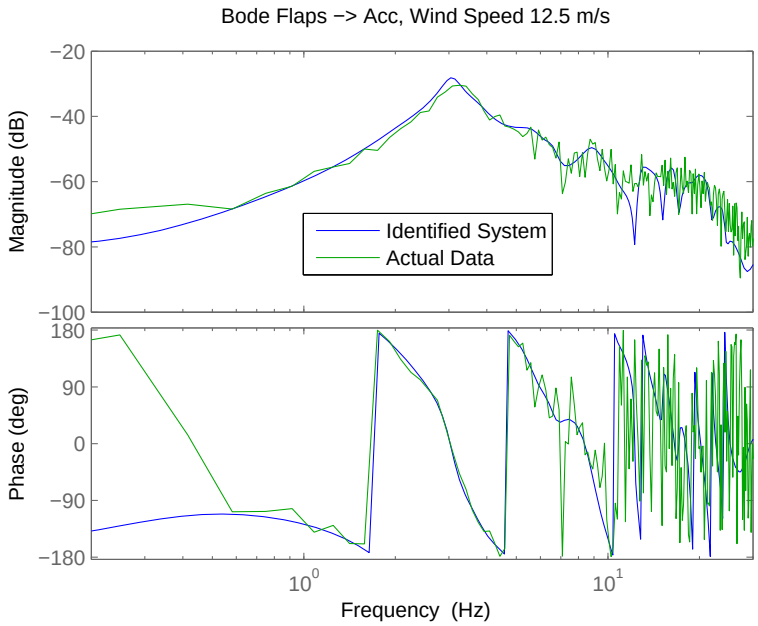

Figure 10: Bode plot of identified system at 12.5 m/s

$$K(s) = K_1(s)K_2(s)K_3(s), \tag{2}$$

where $K_1(s) = k$ is a simple gain, $K_2(s)$ is a phase lead compensator and K_3 is an inverted notch. The filter K_2 adds an adequate amount of phase within the bandwidth to achieve the right amount of damping,

$$K_2(s) = \frac{s/\omega_1 + 1}{s/\omega_2 + 1}, \tag{3}$$

and K_3 enhances feedback at a single frequency, which is the same as the resonance frequency $\omega_r = 3.0Hz$:

$$K_2(s) = \frac{(s/\omega_r)^2 + 2(s/\omega_r) + 1}{(s/\omega_r)^2 + 2\zeta(s/\omega_r) + 1}. \tag{4}$$

The various tuning parameters in the controller equations are detailed in the table below:

Table 3: Control parameters

Parameter	Symbol	Value
Controller gain	k	3.333
Phase lead start frequency	ω_1	0.001 Hz
Phase lead end frequency	ω_2	0.5 Hz
Resonant frequency	ω_r	2.96 Hz
Notch damping	ζ	0.5

When this controller is connected in closed loop with the plant, the structural resonance peak is damped to a large extent, as can be seen in Figure 11. Figure 11 also shows a comparison to the numerical model in both cases 0.5 m/s below flutter speed. In the experiment, the acceleration measurement has been shifted to the pitch axis of the wing instead of being located in the flaps. Therefore the accelerometer does not capture

the flap deflection modes at 1.6 Hz or the pitch mode at 6.8 Hz, which are present in the original data. The amplitude of the plunge mode is almost exactly matched in the numerical model and the experiment. A shift in frequency of the mode however can be observed between the experimental system identification and the numerical prediction. In the experiment the frequencies do not show the same drop with increasing wind speed as was observed in Figure 7 for the instable branch around the flutter point.

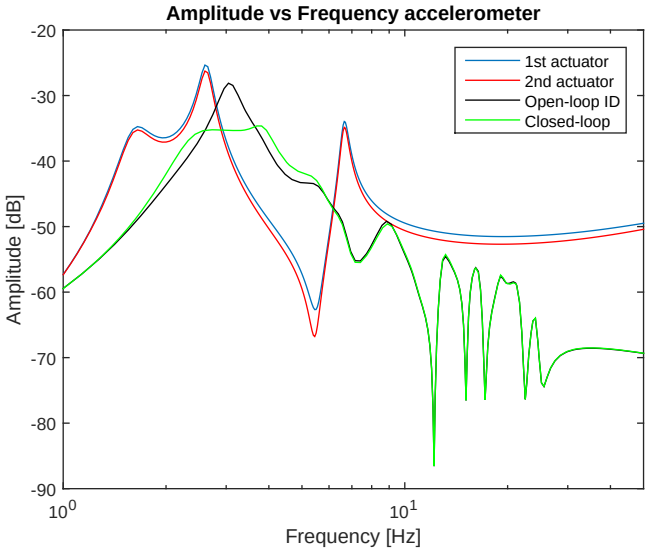

Figure 11: Bode plot of open-loop and closed loop system at 12.5 m/s (experiment) and 10.5 m/s (numerical model)

The increased dmaping of the closed-loop system can also be seen in the time domain simulations shown below, where the eigenmode oscillations decay much fast when the controller is active as shown in Figure 12.

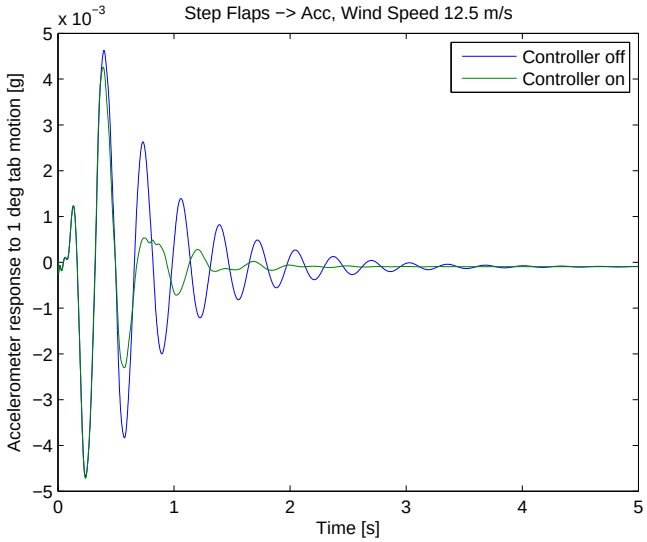

Figure 12: Decay of oscillation: Open-loop versus Closed-loop

VI. Limit Cycle Oscillation

As was pointed out in the introduction, for the energy harvesting it is vital to be close or above the flutter speed. For that purpose, limit cycle oscillations were studied intensively during the experiment. Two

different types of limit cycles were investigated, namely structurally limited cycles and limit cycles that were reach through control of the trailing edge tab. The structural limit was achieved by limiting the maximum deflection of the flaps from -20 to 30 degrees. Figure 13 shows the structurall limited oscillations. The trailing edge tabs were used to initiate the vibration. For small oscillation amplitudes, the system was still stable as a result of non-linear damping.

A sinusoidal oscillation with a frequency of 3 Hz was imposed on the trailing edge tab after 7 seconds. This oscillation immediately caused the flap to rotate at the input frequency. A time delay of 1-1.5 seconds can be observed when comparing the flap oscillations and the acceleration of the plunge mode. This time delay is associated to the mass of the wing, which only slowly starts to oscillate. Practically at the same time as the accelerometer, the load cells, which are connected to the springs, show an oscillation of the forces. In contrast to the load cells, which measure an almost perfect sinusoidal signal, the accelerometers measure a dominant signal of identical frequency but also carry components of the multiples of the frequencies. The damping of the spring system might reduce the amplitude of higher harmonics in the measurements of the vertical forces by the load cells.

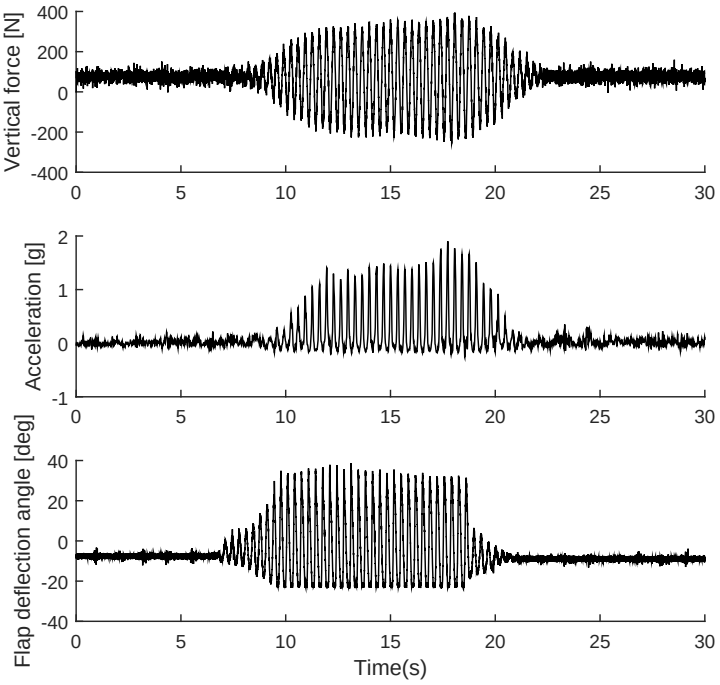

Figure 13: Structurally limit cycle oscillation

From 7.5 seconds until 18 seconds the system is instable and the excitation signal is deactivated. At 9 seconds the flap deflection reaches the delimiters of the flap, which causes a limit cycle oscillation. At 18 seconds the controller is switched on. Almost instantaneously, the amplitude of flap deflections reduces to 10 degrees, from which point it slowly decays. This shows the stabilization effect the trailing edge tabs have on the flaps. The oscillations of the complete system decay slower and reach a static position at 22 seconds.

The second possibility to achieve limit cycle oscillations is to actively use the controller to limit the cycle amplitude. The controller as described above was used, however an on/off condition was included, namely that the controller was only active if the amplitude of the flap deflection over the last oscillation cycle has exceeded a specified threshold. The initialization period of the limit cycle is analogue to the structurally limited oscillations. A sinusoidal oscillation is imposed as seen in the 2nd subfigure of Figure 14. Again, the oscillations starts to grow at which point the excitation signal is stopped. Flutter causes the oscillations to increase until the flaps reach their structural limits. This oscillation is maintained until the controller is activated at 11 seconds. The controller reduces the amplitude of the oscillations. The controller reduces the vibrations of the flaps, but the inertia of the plunge mode is high and its oscillations decay slowly. In that

phase the controller is mostly active until the system has reached a steady state. Around 17 seconds a stable pattern develops. The controller is only active 11 percent of the time. The control activity almost eliminates the vibration of the flaps. Consequently the controller becomes passive. Over a 3-4 of cycles the flutter mechanism increases the flap vibration again until the controller becomes active again and the procedure repeats itself. The inertia of the system causes the accelerations of the wing to decay much slower than the flap deflections when the controller is active. Overall a practically constant limit cycle oscillation is reached at a lower amplitude, with a maximum flap deflection of 15 degree.

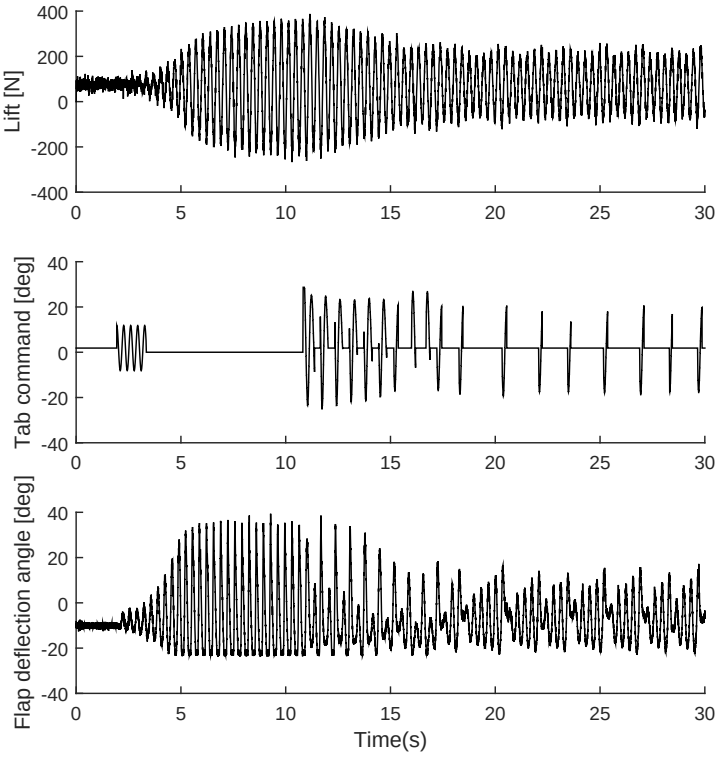

Figure 14: Controlled limit cycle oscillation

VII. Power Balance

The second task of the autonomous, free-floating flap is to generate power in order to be self sustained. As mechanical friction in the system was high, the power that was generated by the flaps could not directly be measured. This mechanical friction is mainly a problem of downsizing the system as small generators need higher rotational speeds than large generators. Consequently, the gear ratio to drive the flaps needs to be very high. A doubling of the generator diameter allows a doubling of the poles and therefore a reduction of the rotational velocities to generate sufficient power. The gearbox also acts as a lever to frictional forces such that even a small friction is amplified to a high resistance torque, which needs to be overcome during flutter. The low test speeds in the wind tunnel dramatically reduce the moment that can be generated to overcome these forces. A full scale wind turbine operates at tip speeds of 60 m/s, compared to the wind tunnel test velocities of around 12 m/s. Additionally, the chord of the wind turbine airfoils close to the tip is 4 times as big as the experimental wing. This results in a moment on the hinge axis that would be 400 times as big as the moment on the wind tunnel model.

The measurements presented in Figure 15 have been obtained by imposing a flap oscillation at the first flutter frequency analogue to the limit cycle oscillations. As can be seen in the 1st subfigure of Figure 15, the frequency of the signals is much higher than the flap oscillation frequency of 3 Hz. This is a result of the

gear ratio. The power signal shows a high noise component. The source of the noise is mechanical friction in the rotation such that a smooth rotation could not be achieved and peaks and drops in the rotational speed are observed. The power that could be reached in the presented configuration was measured over a resistance of 35Ω. Figure 15 displays the sum of all 4 generators that have been installed in the aeroelastic apparatus. The mean power that could be achieve during the equivalent limit cycle oscillations is 0.3133W or a root mean square power of 0.564W.

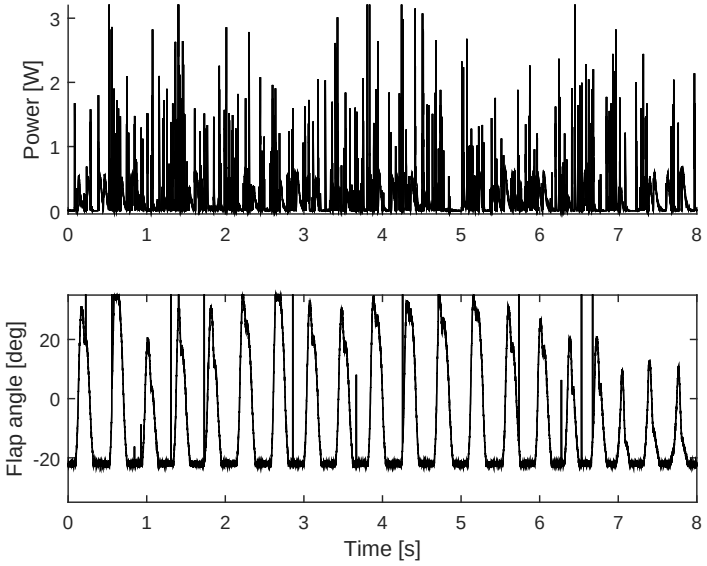

Figure 15: Power production of generators during sinusoidal oscillation at 3 Hz

The harvested energy should be sufficient to power the actuators and the accelerometers. The latter only has a very low power requirement of less than 1mW such that in practice, the driver in power requirement are the actuators that drive the trim tabs. Figure 16 shows an overview of the power consumption of all actuators. The top subfigure displays the current that is drawn for the acutator motion. The actuation system was powered by an external constant voltage source. The voltage that was supplied is as shown in the middle subplot of Figure 16. Up to 4 Hz, the voltage demand could be matched exactly, above a drop in voltage output is observed, however the tabs still remain operational.

The biggest share of the power consumption stems from the operation of the actuators themselves. The additional power requirement by including aerodynamic loads is small compared to the free oscillation. The difference in power is provided in the lower subfigure. This curve includes the difference in power consumption for all actuators combined. Around 3 Hz, this difference is highest at just above 0.4W. However one needs bear in mind that the actuators only need to be active 11.5 percent of the time to fix the limit cycle amplitude. The averaged power consumption due to aerodynamic resistance moments therefore drops to 0.0427W, which is 13.6% of the generated power. When including the actuator power requirements, the average consumption increases to 0.44W, which is 41% higher than the power production, however the actuators were overdimensioned such the trim tab could be actuated even if one of the actuators failed.

VIII. Conclusions

The concept of an autonomous, free-floating flap has been presented and a wind tunnel model designed that was retrofitted into an aeroelastic plunge and pitch apparatus. Numerically, the flutter speed was determined to be 11 m/s, but due to friction in the flap system, the flutter speed was 13 m/s during the experiment. 2 autonomous flaps were installed on a wing. Each system included 2 actuators, 2 generators and an accelerometer. Additional sensors such as load cells were installed on the frame.

During the experiment, the transfer function of the tab command to an accelerometer command was identified. The obtained model matched the numerical model, except for a drop in frequency of the numerical

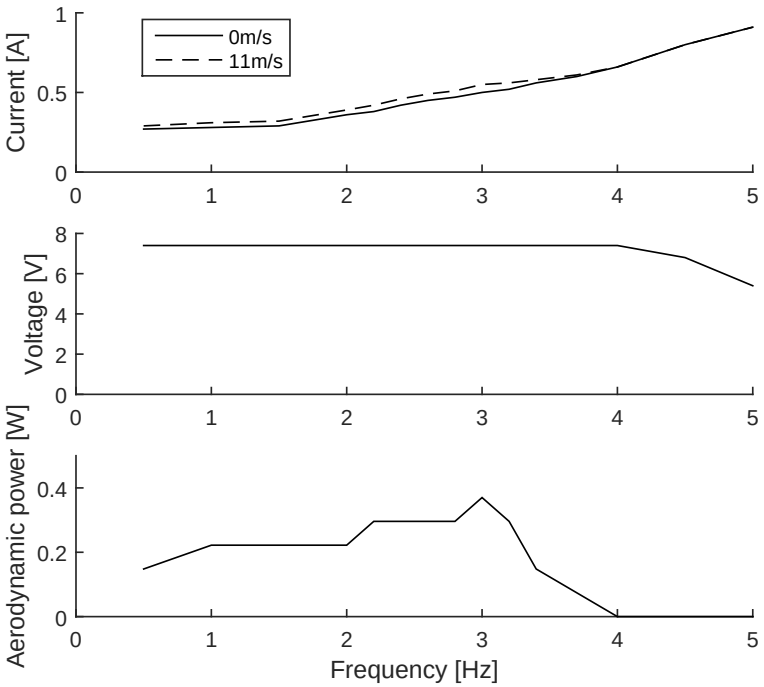

Figure 16: Power consumption of actuation system as function of actuation frequency and wind speed for 20 degree tab amplitudes

model close to the flutter speed, which was not observed during the experiment. The system has been tested in structurally limited oscillations and the controller was used to suppress the flutter mode that was an interaction of the plunge dominated mode and a synchronous flap deflection mode. The controller has been adapted by using on/off conditions to fix the limit cycle amplitude to a given value.

The power of the generators could not directly be measured during the experiment, but an equivalent vibration signal produced and average power of 0.3133W, while the power to overcome the aerodynamic resistance moment was only 0.0427W. Therefore this system could be operated as autonomous unit.

Acknowledgments

This research has been funded by the Far and Large Offshore Wind (FLOW) project of the Dutch Ministry of Economic Affairs.

IX. References

[1]Heinze, S. and Karpel, M., "Analysis and wind tunnel testing of a piezo-electic tab for aeroelastic control applications," *Journal of Aircraft*, Vol. 43, No. 6, 2006, pp. 1799–1804.

[2]Bernhammer, L., De Breuker, R., Karpel, M., and van der Veen, G., "Aeroelastic Control Using Distributed Floating Flaps Actuated by Piezoelectric Tabs," *Journal of Aircraft*, Vol. 50, No. 3, 2013, pp. 732–740.

[3]Pustilnik, M. and Karpel, M., "Dynamic Loads Alleviation Using Active Free-Floating Flaps," *Proceedings of 53rd Israel Annual Conference on Aerospace Sciences*, Haifa, Israel, 2013.

[4]Pustilnik, M. and Karpel, M., "Loads, Vibration and Maneuver Control Using Active Floating Flaps," *Proceedings of International Forum on Aeroelasticity and Structural Dynamics*, Royal Aeronautical Society, Bristol, UK, 2013.

[5]Bernhammer, L., Karpel, M., and De Breuker, R., "Energy Harvesting for Actuators and Sensors using Free-Floating Flaps," *Journal of Intelligent Material Systems and Structures*, Vol. submitted.

[6]Bryant, M. and Garcia, E., "Modeling and Testing of a Novel Aeroelastic Flutter Energy Harvester," *Journal of Vibration and Acoustics*, Vol. 133, 2011, pp. 011010–1:10.

[7]Bryant, M., Fang, A., and Garcia, E., "Self-powered smart blade: Helicopter blade energy harvesting," *Proceedings of the SPIE*, Vol. 7643, 2010, pp. 764317–1:10.

[8]Park, J., Kim, K., Kwon, S., and Law, K. H., "An aero-elastic flutter based electromagnetic energy harvester with wind speed augmenting funnel," *Proceedings of Int. Conference on Advances in Wind and Structures*, KAIST, Seoul, Korea, 2012.

[9]Park, J., Morgenthal, G., Kim, K., Kwon, S., and Law, K. H., "Power Evaluation for Flutter-Based Electromagnetic Energy Harvester using CFD Simulations," *Proceedings of First International Conference on Performance-based and Life-cycle Structural Engineering*, Hong Kong, China, 2012.

[10]Bernhammer, L., Sodja, J., Karpel, M., and De Breuker, R., "Design of an autonomous flap for laod alleviation," *Proceedings of 25nd International Conference on Adaptive Structures and Technologies*, The Hague, Netherlandes, 2014.

[11]Sterenborg, J., *Experimental and numerical investigation of an aeroelastic wing*, TU Delft, 2014, PhD Thesis.

[12]Rodden, W. and Johnson, E., "MSC Nastran Aeroelastic Analysis User's Guide," MSC. Software Corporation USA, 1994.

[13]Zona Technology, "ZAERO Theoretical Manual," Scottsdale, usa, 2011.

[14]Verhaegen, M. and Verdult, V., *Filtering and System Identification: A Least Sqaures Approach*, Cambridge, UK, Cambridge University Press, 2007.

[15]Chiuso, A., "The role of vector auto-regressive modelling in predictor based subspae identification," *Automaticay*, Vol. 43, 2007, pp. 1034–1048.